A combined in-situ and post-mortem investigation on local permanent degradation in a direct methanol fuel cell

F. Bresciani [a], C. Rabissi [a], M. Zago [a], P. Gazdzicki [b], M. Schulze [b], L. Guétaz [c], S. Escribano [c], J.L. Bonde [d], R. Marchesi [a], A. Casalegno [a, *]

[a] *Politecnico di Milano, Department of Energy, via Lambruschini 4, 20156 Milano, Italy*
[b] *German Aerospace Center (DLR), Institute of Engineering Thermodynamics, Pfaffenwaldring 38-40, 70569 Stuttgart, Germany*
[c] *CEA, LITEN, 17 rue des Martyrs, 38054 Grenoble, France*
[d] *IRD Fuel Cell A/S, Emil Neckelmanns Vej 15 A&B, DK-5220 Odense, Denmark*

Received 21 July 2015
Received in revised form 24 November 2015
Accepted 27 November 2015 Available online 13 December 2015

1. Introduction

The direct methanol fuel cell (DMFC) technology is a promising energy source for portable and automotive applications, mainly due to the direct use of a liquid fuel, quick recharging and low operating temperature [1–3]. In the last decades the research activities on DMFC have been mainly focused on the development of innovative materials in order to improve performance [4–7], as, for example, reducing methanol crossover [8,9] and increasing the effectiveness of the catalysts [10,11]. However, further critical issues still must be overcome to reach market competitiveness, among which severe performance degradation is one of the most relevant [12–15]. Therefore, the number of experimental investigations of DMFC degradation is continuously increasing [16–20] and recently a

* Corresponding author.
E-*mail address:* andrea.casalegno@polimi.it (A. Casalegno).

thorough review has been published [21].

DMFC performance loss can be partially recovered by interrupting the operation for diagnostics or by using appropriately developed procedures. Cha et al. characterize this behaviour defining a permanent and a temporary contribution [22], but the latter is not definitely explained. Several studies attribute the performance recovery to the cathode, probably due to the reduction of platinum oxides [23] or to the removal of water accumulation (i.e., flooding) [24]. Instead, other studies propose the galvanic/electrolytic operation of the DMFC as temporary degradation mechanism, due to hydrogen generation at the anode side [25,26]. These works [23–27] demonstrate that an interruption of both operation and cathode air feeding determine a positive effect on DMFC performance. For this reason, the focus on operating strategies that allow reducing temporary degradation mainly regards DMFC cathode [28,29]. Instead, temporary degradation of the DMFC anode has been firstly identified in Refs. [30], where it has been attributed to CO_2 accumulation in both catalyst layer (CL) and gas diffusion layer (GDL), as confirmed by the reduction of methanol crossover during degradation tests [31]. However, DMFC temporary degradation minimization is not extensively investigated in the literature since permanent and temporary contributions are not effectively distinguished.

In the literature, permanent degradation is attributed to both the electrodes and to the membrane and different degradation mechanisms are highlighted. Electrochemical surface area (ECSA) loss can be due to phenomena such as platinum dissolution, ruthenium dissolution and crossover and carbon corrosion [16–18], while membrane delamination and thinning are sometimes highlighted as other mechanisms. However, permanent degradation itself is seldom identified [22] from the temporary one and its quantification is not performed in standard and repeatable operating conditions.

DMFC shares some permanent degradation mechanisms with hydrogen polymer electrolyte membrane fuel cell (PEMFC), like typical platinum degradation mechanisms involving an average catalyst particle size increase, such as dissolution and re-deposition [17,22,32,33], highlighted for example by X-ray diffraction (XRD) and transmission electron microscopy (TEM) observations. Moreover, membrane degradation due to pinholes, crystallinity increase [13,32] seems to occur mainly next to the cathode side [17], while GDL degradation is mainly investigated with scanning electron microscopy (SEM) and energy dispersive X-ray spectroscopy (EDS) showing a general polymer loss [19,34]. Among the main DMFC degradation mechanisms, the literature focuses on the instability of the ruthenium nanoparticles resulting in ruthenium dissolution and crossover to the cathode investigated mainly through EDS [17,28,35]; however, no work presents the investigation of the heterogeneities related to the different DMFC permanent degradation mechanisms in the different regions such as reactants inlet and outlet, while a deep focus on the degradation heterogeneities in PEMFC has been already presented in Refs. [33,36]. Moreover, the coupling between the measurements obtained during the DMFC operation and the post-mortem analysis is seldom carried out [28]. From the literature analysis emerges that a direct relation between each degradation mechanism and the corresponding voltage decay is missing, as also highlighted in Ref. [21].

The aim of this work is to separate and quantify the effect of each component degradation on voltage decay. Periodic in-situ diagnostic measurements, assisted by modelling analysis, allow to distinguish the effects of active area loss at both at anode and cathode, mass transport issue, membrane decay and reversible degradation. Ex-situ analyses on pristine, activated and aged components (with in-plane and through-plane local resolution) allow to identify the major degradation mechanisms and the related heterogeneities. Finally, the consistency of the results from in-situ and ex-situ analyses are discussed in details to provide a further insight on DMFC degradation.

2. Experimental methodology

2.1. DMFC sample and experimental setup

The DMFC membrane electrode assemblies (MEAs) used in this work, both for the preliminary tests on *full refresh* procedure and for the long term test, are commercial 25 cm^2 manufactured by IRD Fuel Cell A/S. The membrane is Nafion® 115, anode catalyst loading is 1.8 mg cm^{-2} (PtRu) and cathode catalyst loading is 1.2–1.4 mg cm^{-2} (Pt). Both anode and cathode diffusion layers are Sigracet® SGL35DC (thickness 325 μm, 20% PTFE content, with microporous layer (MPL)). Nominal current density is 0.25 A cm^{-2} and fuel cell temperature is maintained at 75 °C. During testing, unless differently indicated, anode and cathode are fed respectively with 1.0 M methanol solution (with stoichiometry equal to 6 at nominal current density) and air, saturated by water at ambient temperature (with stoichiometry equal to 3 at nominal current density).

The experimental setup utilized in this work is explained in detail in Ref. [37].

2.2. Operating strategy description

As explained in Refs. [31,38], a DMFC cannot work in continuous operation due to an excessive degradation rate and consequently they are usually operated by means of discontinuous operating strategies. For the long term degradation test, the DMFC has been operated by cycles of 20 min followed by 1 min of *refresh* cycle. About every 120 h of operation, an interruption for diagnostic is performed to evaluate permanent degradation.

The *refresh* cycle is an IRD Fuel Cell confidential procedure that consists of a sequence of OCV and cathode air feeding interruption,[1] similar to that reported in Ref. [24], which allows recovering the temporary degradation. In the *refresh* cycle, as the air feeding is switched off, cathode potential drops to less than 0.3 V and when the operation restarts a significant positive effect on performances is obtained. A preliminary interpretation of the positive effect of *refresh* cycles on DMFC performance has been already presented in Refs. [29,39], where temporary degradation turned out to be caused on one end by a gradual increase of CO_2 content in the anode porous layers that hinders reactant transport to active sites, on the other hand by Pt oxides formation in the cathode catalyst layer due to operation at high cathode potential. The refresh cycle proposed in Ref. [29] permits to lower the CO_2 content at the anode inter-rupting its operation while flowing the reactant and to reduce the Pt oxides at cathode lowering its potential thanks to an interruption of air feeding. However, despite this operating strategy results in a lower temporary degradation than the one occurring during continuous operation, it does not entirely eliminate the temporary decay. Therefore, a *full refresh* procedure, able to fully recover temporary degradation, has been developed and utilized before carrying out diagnostic measurements. The details are reported in Appendix A1.

2.3. In-situ electrochemical diagnostic measurements

The following diagnostic measurements have been periodically performed to characterize permanent degradation, once the

[1] The details cannot be provided for confidential agreement.

temporary contribution has been recovered by means of *full refresh*:

- Polarization curve with mass transport analysis

The acquisition is composed of 9 single measurement points referred to different current densities, collected following one-way curves increasing current. Each single acquisition point is performed at constant current, measuring voltage and current for 600 s. The data obtained from each single acquisition point are elaborated as explained in Ref. [37]. Each polarization curve is performed with reactants at constant flow rates, in order to ensure the steady state operation determining the high reliability of methanol crossover and water content in cathode outlet measurements. However, it should be noted that the voltage values obtained from the polarization curves, especially at high current densities, are affected by temporary degradation resulting in lower values if compared with the ones obtained during the degradation test, as highlighted in section 3.2.

- Electrochemical Impedance Spectroscopy (EIS)

EIS are performed at 0.1 and 0.25 A cm^{-2} during the diagnostic polarization curves using a Potentiostat/Galvanostat (Autolab PGSTAT 30) provided with a frequency response analysis (FRA) module, as detailed in Ref. [30]. The impedance is measured at 50 frequencies included between 10 kHz and 50 mHz with a logarithmic distribution. Measurement consistency is verified by a retrospective use of Kramers-Kronig transforms [40,41]: the impedance values that do not satisfy such relations are not considered meaningful.

- Cathode Cyclic Voltammetry (CV)

CV is used to estimate the cathode ECSA. Hydrogen (3.5 Nml min^{-1}) and fully humidified nitrogen (0.6 Nl min^{-1} saturated at 80 °C) are fed to anode and cathode compartments, respectively. Anode is taken as reference and counter electrode, while cathode is taken as working one; its potential is continuously scanned back and forth between 0.05 V and 0.6 V with a speed rate of 25 mV s^{-1}. The cathode ECSA is estimated considering the pos-itive current density peak related to the hydrogen desorption [42]. The estimation is done assuming that the cathode catalyst is covered by a monolayer of hydrogen with a charge density of 210 μC cm^{-2}.

- Linear Sweep Voltammetry (LSV)

LSV is a common diagnostic tool for PEMFC [43], which has been adapted to DMFC diagnostic. It permits to quantify the hydrogen crossover through the membrane and the membrane electric resistance, which are useful proxy to investigate the membrane aging (such as pinhole formation or short-circuit development) in DMFC as well. During this measurement, hydrogen is supplied to the anode (3.5 Nml min^{-1}) and 80 °C saturated nitrogen is supplied to the cathode (0.6 Nl min^{-1}), as done for the CV. The LSV consists in linearly rising the cathode potential over the anode one from 0.085 V up to 0.55 V with a speed rate of 1 mV s^{-1}, so that the hydrogen adsorbed on the cathode catalyst [37] is progressively oxidized. The current related to the hydrogen oxidation is measured as indication of the hydrogen crossover rate [42], while the short circuit current across the membrane is estimated considering the current/voltage ratio when increasing current. Thus, the LSV results can be used as diagnostic tools for membrane degradation.

- Anode polarization curve

The anode polarization curves have been performed during the investigation, in order to characterize the anode contribution to the permanent degradation, with the same methodology discussed in Ref. [30], where cathode is fed with hydrogen and behaves as a dynamic reference electrode (DHE).

2.4. Ex-situ post-mortem analyses

- X-ray Photoelectron Spectroscopy (XPS)

XPS measurements have been performed using a Thermo Scientific ESCALAB 250 ultra-high vacuum (UHV) facility with a base pressure of 1×10^{-9} mbar. As X-ray source an Al/Mg twin-anode (Thermo Scientific XR4) was used operated at 300 W. As a detec-tor was used a hemispherical electron energy analyser operated in a large area mode with an analysed surface area of 50 mm^2.

In tape peel-off depth profiling experiments, the adhesive tape (3 M Scotch®) is pressed onto the sample. Then, the upper sample layer is removed by peeling off the tape; eventually, the sample is analysed by XPS. Details of this approach are reported in Ref. [44]. According to gravimetric measurements the thickness of the peeled-off material of CL and MPL corresponds to (4.2 ± 1.8) μm and (0.5 ± 0.2) μm, respectively (assuming a mean density of the ma-terials of 1 g cm^{-3}, density of MPL). In contrast to XPS depth profiles performed using ion etching, the peel-off technique is chemically non-destructive.

The concentrations of elements (given in atomic percent, at%) occurring in the studied samples were quantified using sensitivity factors provided by Thermo Scientific using Shirley algorithm for peak background correction. The samples have been analysed as-received. For the analysis of the CL/MPL interface the MEAs were kept in di-water for several days; after this process the two layers could be disassembled easily by slightly pulling the GDL off the membrane.

As reference sample an activated DMFC MEA operated for 30 h (duration of the activation procedure to reach Begin of Life performances, BoL) was used.

- Transmission Electron Microscopy

Thin MEA cross-sections were prepared in order to observe the microstructure by TEM. These thin sections were cut from the embedded MEA using a LEICA ultramicrotome. TEM analyses have been performed on a JEOL 2000FX microscope equipped with EDS (energy dispersive X-ray spectroscopy) system. The use of the last generation analytical TEM (FEI-OSIRIS), provided the possibility to perform accurate chemical analysis with a very good spatial resolution (around 0.1 nm). For the aged MEA, the microstructure degradation was studied in two surface regions selected following previous studies [33]; the first one located near the reactants inlet and the second one near the reactants outlet, since ageing tests were performed in co-flow operation.

3. Long term degradation test

Fig. 1 reports the DMFC voltage behaviour during the long term test performed at constant current and stoichiometry. As anticipated in paragraph 2.2, this test consists in cycles of about 120 h of operation, interrupted by a diagnostic break preceded and followed by a *full refresh*. Temporary degradation recovery is evident after each diagnostic test, moreover an increase of temporary degradation rate is observable during the test. Further study is necessary to provide an explanation of such behaviour.

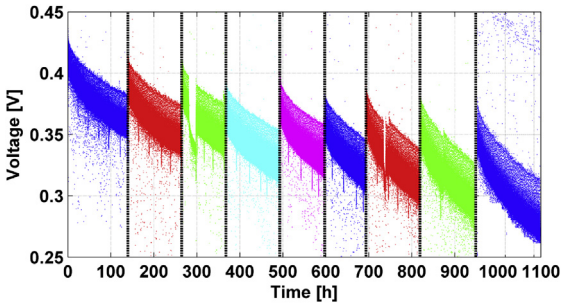

Fig. 1. Voltage decay during the long term test performed at 0.25 A cm^{-2}. Each performance recovery corresponds to the operation interruption for diagnostic with full refresh; the scatter points below and above the cell voltage are due to the voltage sweep during the refresh cycles.

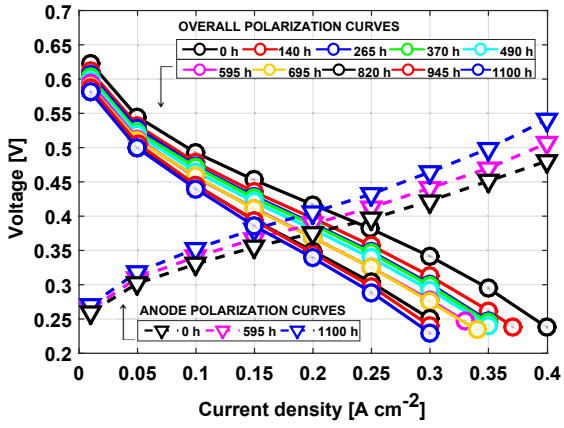

Fig. 2. DMFC and anode (V vs DHE) polarization curves performed during the long term test.

Fig. 2 shows the evolution of polarization curves during the long term test. Two main features can be pointed out: a progressive downward translation, already noticeable at low current densities, and a progressive change of the polarization curves slope. Anode polarization curves are performed only at the beginning, middle and end of life (EoL), in order to provide quantitative information on the anode electrode performance evolution. For the sake of shortness neither voltammograms nor impedance spectra are reported, while a complete results discussion is provided in the followings.

3.1. Degradation analysis at 0.01 A cm^{-2}

DMFC permanent degradation is evaluated considering the voltage decay at a current density equal to 0.01 A cm^{-2} immediately tested after the *full refresh*. At low current density, the overpotentials associated to ohmic and mass transport losses are negligible, as well as temporary degradation: hence the voltage decay represents the permanent degradation and is mainly caused by ECSA loss.

From Fig. 2 it is possible to calculate a permanent degradation due to ECSA loss equal to 9 μV h^{-1} and 31 μV h^{-1} for anode and cathode electrode, respectively, leading to an overall degradation of

[2] Since the anode voltage loss in time at 0.01 A cm^{-2} is limited, a linear regression between the 3 measured anode voltage has been performed to evaluate its value in time. The cathode potential decay is thus calculated as the sum between the cell voltage and the anode voltage.

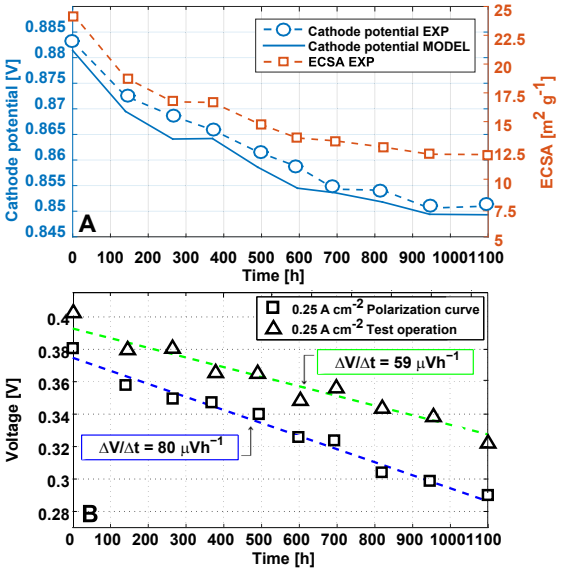

Fig. 3. Comparison between cathode ECSA and cathode potential decay at 0.01 A cm^{-2} (A) and between voltage values in reference conditions (0.25 A cm^{-2}) measured from the polarization curves and long term test just after diagnostic break (B).

about 40 μV h^{-1}. Therefore, the effect of ECSA loss is predominant at the cathode electrode.

Fig. 3A reports a comparison between the calculated cathode potential decay[2] at 0.01 A cm^{-2} and the cathode ECSA measured from the CV.

An ECSA non-linear decay with a strong initial decrease is evident, which is consistent with the typical platinum degradation mechanisms reported in the literature [45], i.e. Pt dissolution and Ostwald ripening. The long term test shows a reduction of about 50% of cathode ECSA from the BoL value in about 1100 h. Indeed, during DMFC operation, cathode electrode works in strongly degrading conditions, such as very high potentials and high water content and flux, enhancing platinum ion transport and platinum dissolution.

In order to support quantitatively the above mentioned considerations, the cathode potential decay associated to ECSA loss is calculated utilizing a 1D+1D DMFC model [46], which considers both kinetic and mass transport losses through the CL thickness [47]. The model has been validated at the same time with respect to different typologies of measure: anode polarization, complete polarization, methanol crossover and water content measured at cathode outlet. In this way all the main physical phenomena are described with a limited uncertainty: a similar approach has been already presented in Ref. [48]. For the sake of shortness in this work the complete comparisons between simulated and measured data are not reported.

The cathode ECSA loss reported in Fig. 3A has been introduced in the model to simulate cathode potential evolution. Model predictions in Fig. 3A are consistent with the experiments and confirm that the voltage evolution at 0.01 A cm^{-2} is representative of the permanent degradation related to ECSA loss.

3.2. Degradation analysis at 0.25 A cm^{-2}

The performance loss in the polarization curves at the reference current (i.e. 0.25 A cm^{-2}) results in a degradation equal to 30 μV h^{-1} and 50 μV h^{-1} for anode and cathode, respectively. This leads to an overall degradation of about 80 μV h^{-1}, Fig. 3B.

These degradation values are considerably higher than the corresponding ones previously evaluated at 0.01 A cm^{-2}. Probably this could be related to the accumulation of temporary degradation acquiring the polarization curve, since no refresh cycle is performed: the nominal operating current of 0.25 A cm^{-2} is reached after one hour.

On the contrary, during long term operation, the voltage just after diagnostic test is not affected by temporary degradation, so the voltage decay, reported in Fig. 3B, represents the permanent degradation, equal to 59 μV h^{-1}.

The difference between these two calculation methods is attributable to temporary degradation effects and turns out to be equal to 21 μV h^{-1}.

The overall permanent degradation evaluated from long term operation (59 μV h^{-1}) is higher than the one related to ECSA reduction evaluated at 0.01 A cm^{-2} (40 μV h^{-1}). The 19 μV h^{-1} difference must be related to other degradation phenomena, which will be analysed in the following sections.

3.3. Membrane degradation analysis

Fig. 4A–D report the results of diagnostic techniques used to investigate polymer electrolyte membrane degradation, including both electrochemical and mass transport measurements obtained during the polarization curves. Methanol crossover acquired at nominal current density, reported in Fig. 4A, does not highlight significant modifications in time. Water content at cathode outlet, in Fig. 4B, remains about constant, suggesting that membrane mass transport properties do not observe considerable changes. However, methanol crossover and water content at cathode outlet are regulated by the interaction of very complex transport mechanisms [46,49] and the degradation of a single component (i.e. GDL, MPL, CL or membrane) does not inevitably result in a significant alteration of DMFC mass balances, unless it is the limiting one.

Membrane ohmic resistance can be measured through the EIS performed during the diagnostic polarization curves. The real axis intercept at high frequency (about 1–5 kHz), detailed in Fig. 4C, does not highlight significant changes over test time. From Ohm's

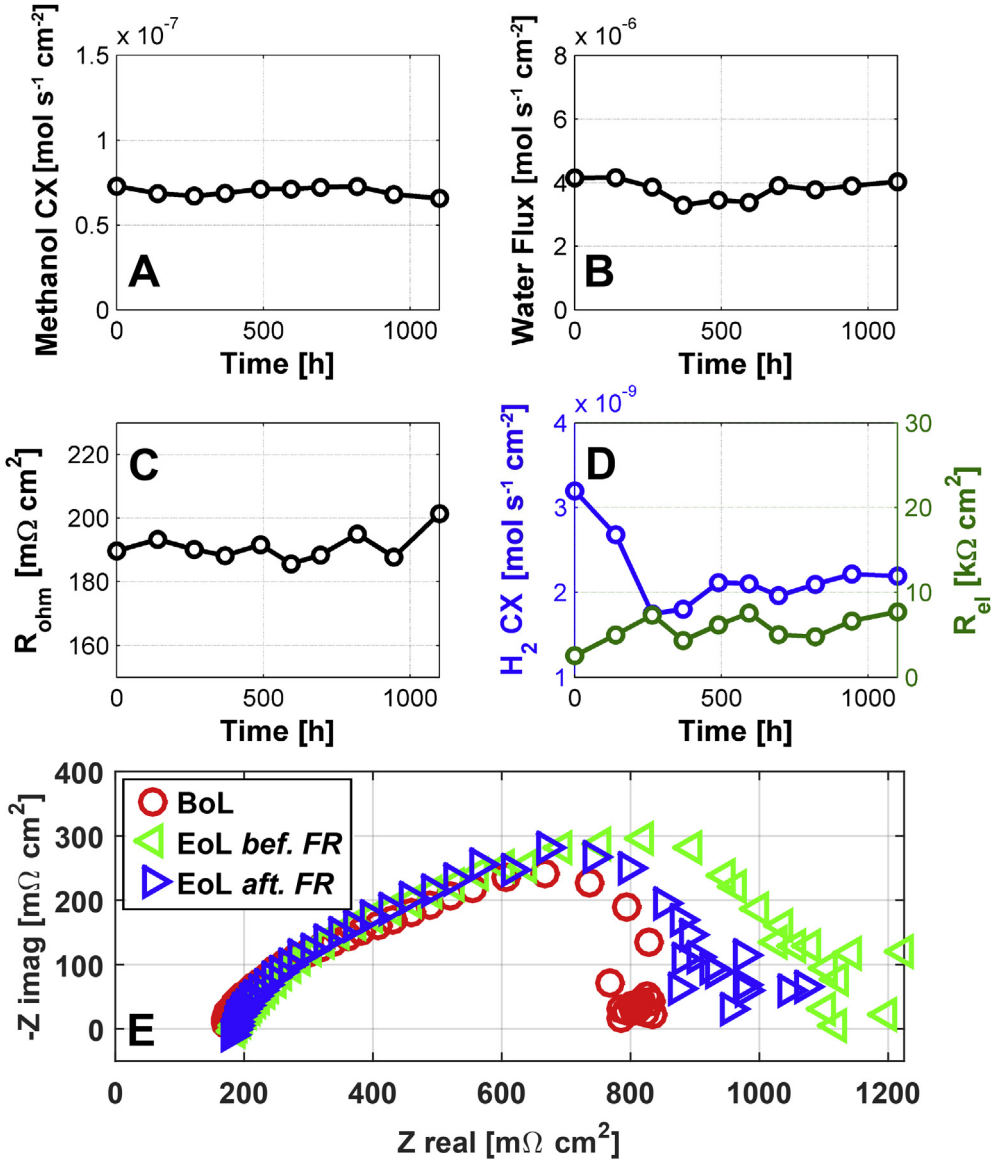

Fig. 4. Methanol crossover (A) and water content (B) in cathode outlet at 0.25 A cm^{-2} during the polarization curves; membrane ohmic resistance obtained from EIS (C) and electrical resistance together with hydrogen crossover obtained from LSV (D); EIS spectra at BoL and EoL before and after the last full refresh (E).

law it is possible to quantify the permanent degradation attributable to the membrane at reference current: it turns out to be about 4 $\mu V\ h^{-1}$ out of 59 $\mu V\ h^{-1}$, a minor contribution compared to anode and cathode electrode degradation.

3.4. Electrochemical impedance spectroscopy analysis

The previous sections highlighted that nearly 15 $\mu V\ h^{-1}$ of permanent degradation (59 $\mu V\ h^{-1}$) occurring at 0.25 A cm^{-2} are not related to neither ECSA loss (9 + 31 $\mu V\ h^{-1}$) nor membrane degradation (4 $\mu V\ h^{-1}$). This loss could be related to mass transport issues within the catalyst and the diffusion layers.

EIS is the most common in-situ technique which permits to separate kinetic and mass transport losses occurring in the system. In this work impedance spectra have been systematically performed during the long term test and the diagnostic breaks in order to monitor the evolution of DMFC internal losses.

Fig. 4E shows the DMFC impedance spectra measured at BoL and EoL before and after the last test *full refresh*. At EoL a reduction of the total resistance is noticeable after the *full refresh*, consistently with the performance recover. Instead, comparing the EIS at BoL and EoL after *full refresh* two main features can be pointed out: an increase in cathode capacitive feature consistent with cathode ECSA loss and a mass transport effect in the low frequency region. The increased mass transport resistance can be caused by a permanent variation of mass transport properties of catalyst or diffusion layers, but can also be explained by an heterogeneous ECSA reduction that determines an increment of current and reactant flux in the healthiest region of the MEA, as reported in Ref. [50]. Post mortem analyses, presented in the following sections, reveal which components are responsible for such impedance modification.

4. XPS results

This section contains the XPS analysis of the MEA components: GDLs, MPLs and CLs.

4.1. XPS analysis on the degradation of catalyst material

In order to analyse the MPL/CL interfaces of the DMFC MEAs peel-off depth profiles, measured with XPS, have been performed.

The depth profiles of the catalyst material in the pristine, the activated and the 1100 h aged samples plotted as atomic percentages versus peel-off steps are depicted in Fig. 5. The images comprise data measured at the anodic as well as cathodic MPL/CL interface. In order to concentrate on the degradation of the catalyst material, only data of Pt and Ru is considered in the plot. Data of carbon (C1s), fluorine (F1s) and oxygen (O1s) are not shown: in the MPLs their concentration are ~60 (C), ~40 (F), and ~1 at% (O); in the CLs the corresponding values equal ~50 (C), ~45 (F), and ~3 at% (O). The spectra are well understood and are described in detail elsewhere [44,51–54].

The main difference between the anode and the cathode CL of the pristine MEA is that on the anode side both Pt (0.6 at%) and Ru (0.4 at%) are observed as catalysts. The cathode CL, on the other hand, contains 1.6 at% Pt as the only catalytically active element.

Regarding the activated and aged MEA the main observations are: (i) in the anode MPL, only Ru is observed and it occurs only in the inlet zone upon aging; (ii) in the aged anode CL less Pt in the inlet is observed compared with the activated MEA; (iii) the aged cathode CL contains slightly less Pt than the pristine and activated MEA; (iv) on the cathode side Ru appears already after activation; (v) in the cathode MPL there is significant amount of Pt observed after aging after the 1st peel-off step.

The significant amounts of Ru in the cathode CL of the activated and aged MEA are likely due to crossover from the anode side. The atomic concentration of the crossed over Ru is in the range of 0.1–0.2 at% which is in agreement with values published in the literature [55,56]. As the concentration of crossed-over Ru is only slightly higher in the aged MEA than in the activated MEA, it is concluded that this process mainly occurs during the activation phase of the fuel cell and it proceeds very slowly upon long time operation. The initial strong degradation of the catalyst is in accordance with the initial strong cathode ECSA loss observed through the CVs, already shown in Fig. 3A. Hence, the Ru crossover effect is not expected to significantly contribute to the performance loss of the fuel cell after long time operation.

In this context it is noted that the mean cathodic Ru concentration in the aged MEA is similar in the air outlet zone (0.16 ± 0.04 at%) and in the air inlet (0.11 ± 0.02 at%).

Interestingly, in the 1100 h aged anodic MPL substantial amounts of Ru are observed in the fuel inlet zone, suggesting a diffusion of Ru from the anodic CL to the MPL/GDL. However, it is yet unknown why only the gas inlet zone is affected by this Ru redeposition in the MPL/GDL region. Thereby, the concentration of anodic Ru is not reduced in the aged anode CL, suggesting that the amount of dissolved Ru is rather low, or that Ru dissolves from areas that are not accessed experimentally (deep layers). It is noted that even at the GDL back side ~0.1 at% Ru has been detected. This effect is not observed in the activated MEA.

The detailed Pt4f and Ru3p spectra of the pristine and aged catalyst layers (not shown) do not exhibit any significant changes in peak shape or position, suggesting that the chemical state of pris-tine Pt and aged Pt as well as between anodic Ru and crossed Ru are likely the same. For Pt a similar finding is reported in other XPS studies [56].

For the aged MEA, the Pt concentration is reduced by 30% compared to the pristine MEA. A mechanism that would lead to such a finding is the covering of cathodic Pt particles by the migrated Ru. As will be discussed later, a comparison of XPS and X-EDS results supports the idea of the coverage of Pt by Ru. Additionally, an agglomeration of Pt, i.e. a substantial growth of particle size associated with a reduction of particle number, would lead to a similar observation too. According to TEM measurements presented in section 5, a clear increase of particle size after operation could not be unambiguously confirmed.

4.2. XPS analysis on the degradation of carbon and polymers in the CL and MPL

Another change observed in the CL as well as in the MPL, due to fuel cell operation, is the loss of the polymer concluded from the C1s details spectra of the CL and the MPL shown respectively in Fig. 6A and B. The plots show normalized spectra of carbon containing species in the pristine, the activated and the 1100 h aged sample. In the case of the aged MEA, the inlet and the outlet regions have been analysed to verify degradation heterogeneities. In both panels the two main peaks are due to carbon within the carbon black (284 eV) and carbon bound in the polymers (292 eV), i.e. PTFE in the case of the MPL and the ionomer in the case of the CL [54–59]. The shoulder at 281 eV is the overlapping signal due to the $Ru3d_{5/2}$ level of ruthenium. The ratios of the amount of carbon in the carbon black and the carbon bound in the polymer (ionomer or PTFE) $C_{carbon\ black}/C_{polymer}$ calculated from the peak areas and shown in Fgiure 6C and 6D, clearly suggest that the increase of $C_{carbon\ black}/C_{polymer}$, attributed to a loss of the binder polymers within the CL or PTFE within the MPL, occurs fast during the beginning of operation of the MEA and proceeds slowly upon further (long time) operation as substantial changes are already

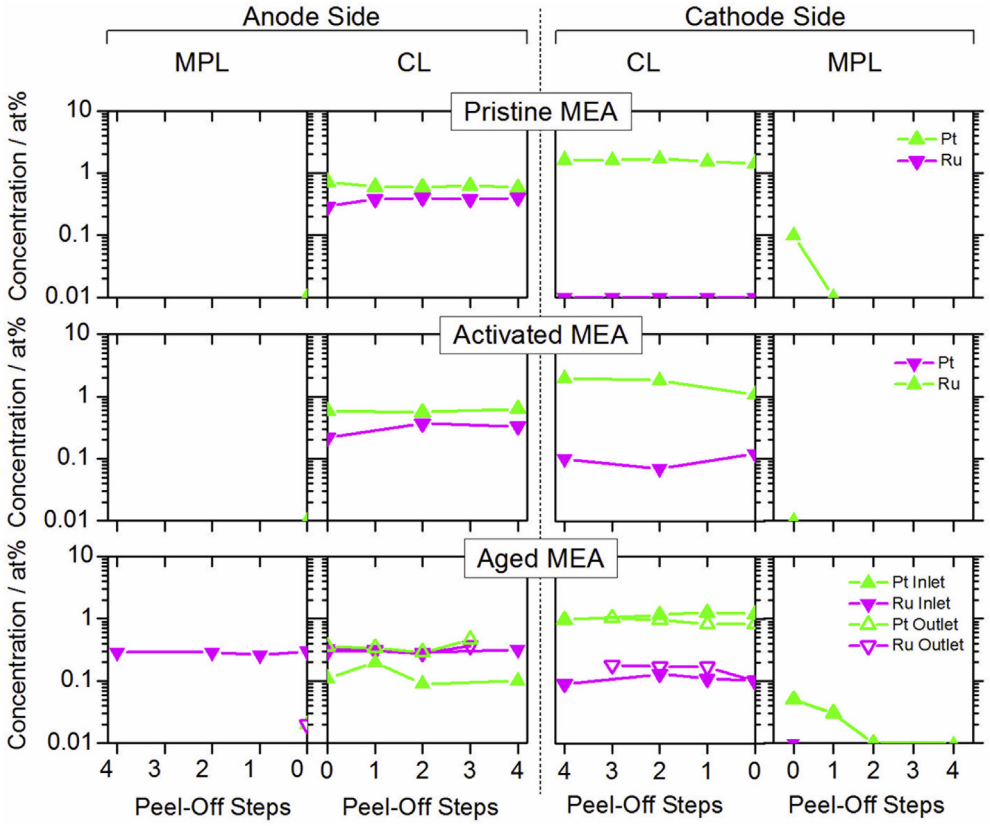

Fig. 5. Peel-off depth profiles of the anode and cathode side MPL/CL interfaces of the pristine, activated (30 h operation) and aged MEA (1100 h operation). In the case of the aged MEA the solid and open symbols correspond to the inlet and outlet zone of the flow field, respectively.

observed after 30 h of operation. This observation points out the great impact of the activation procedure.

It is noted that the observed trends are the same on the anode and on the cathode side. Moreover, for both the CL and the MPL, for the 1100 h aged MEA there are no significant differences between the inlet and outlet zones.

The loss of polymers in these layers may lead to several different effects related to a performance loss of the cell, such as a poor ionic conductivity within the CL, a decrease of the active surface area (reduced catalyst/ionomer interface), or an increase of the electrical cell resistance due to reduced connection of catalyst and carbon.

Finally, it is worth to mention that the ratio of $C_{polymer}/F_{polymer}$ does not change upon operation for both the CLs and the MPLs suggesting that loss of PTFE in the MPL and of ionomer in the CL cannot be associated with a chemical degradation based on these results (in contrast to GDLs, see next section).

4.3. XPS analysis on the degradation of the GDLs

In Fig. 6E and 6F, XPS spectra of the C1s region of GDL anode and cathode back sides of the pristine, the activated and the aged MEAs are shown. The spectra exhibit three major peaks due to carbon fibres (284 eV), carbon bound in the PTFE (292 eV) [54,59,60], and carbon within electrically charged PTFE (298 eV) caused by ionization by the X-rays [53].

Beside changes of the relative intensities of the peaks at 292 and 298 eV, attributed to structure changes such as wetting or dewetting of the carbon fibres by PTFE (not further discussed here), a major finding is the chemical degradation of PTFE especially in the anodic GDL: specifically, in the spectrum of the anodic GDL of the aged MEA a new peak emerges at 288 eV that is not observed in spectra of the other samples. This peak is typical for carbon in a CF-C compound [61] taken as an evidence for fluorine depleted PTFE. An analogous effect, yet significantly less pronounced, is suggested to occur in the aged cathodic GDL too as concluded from the increased intensity between the peaks at 284 and 292 eV.

5. TEM results

SEM (Scanning Electron Microscopy) and TEM analyses were performed on a fresh MEA and on the aged MEA after long time (1100 h) operation; SEM images are not reported for sake of the shortness; anyway, the aged MEA cross-section analysis did not reveal severe degradation of the global microstructure, especially no apparent membrane degradation or thinning was detected. The high variance in the electrodes thickness did not permit one to appreciate significant differences between the fresh and the faded MEA.

The ultramicrotomy preparation of thin cross-section permitted to study by TEM the different components of the DMFC in different zones such as reactants inlet and outlet.

5.1. TEM analysis on the fresh MEA

Regarding the fresh MEA TEM analysis, not reported here for the sake of shortness, a slight heterogeneity has been identified already in the pristine component structures, where agglomerates of different darkness have been observed. In the cathode, the size distribution of Pt catalysts is between 3 and 8 nm in the darker agglomerates whereas it is around 2 and 4 nm in the brighter agglomerates; the larger Pt nanoparticles generally are near the agglomerate surface. It is also worth noting that large Pt

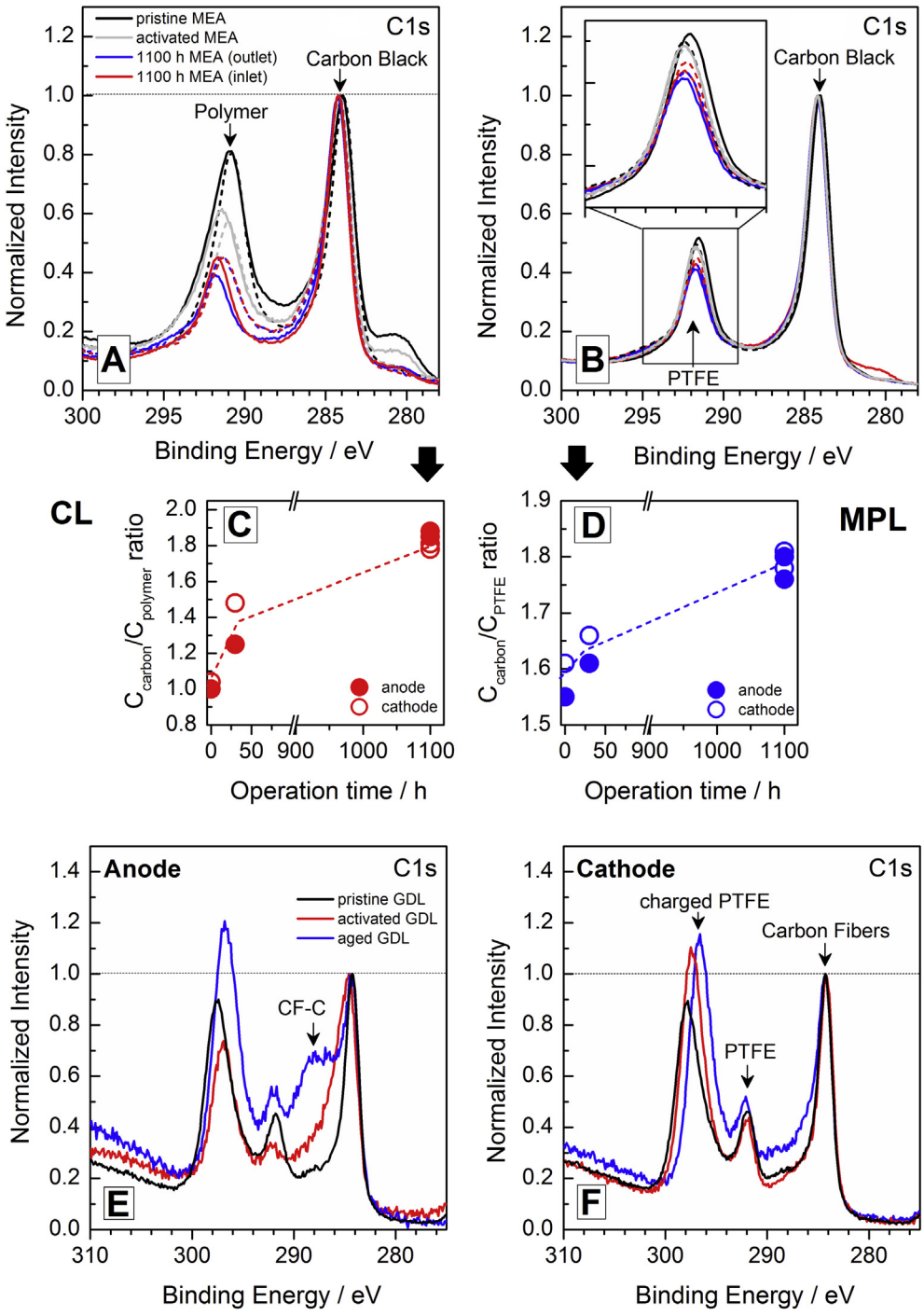

Fig. 6. XPS spectra of the C1s regions of the pristine, activated and 1100 h aged catalyst layers (A) and microporous layers (B) (solid and dashed lines correspond to the anode and the cathode side, respectively), Anode GDL (E) and Cathode GDL (F). The spectra are normalized with respect to the intensity of the 284 eV peak. Detail of $C_{carbon\ black}/C_{polymer}$ ratio in CL (C) and MPL (D) versus operation time.

agglomerates (more than 1 μm large) can be observed in the cathode.

In the anode of the fresh MEA, we could observe a large variation of grey levels between the agglomerate images corresponding to large variation of Pt–Ru nanoparticles distributions. The range of particle size is around 2–5 nm for the darker particle and around 1–3 nm, with few 10 nm large nanoparticles for the brighter agglomerate. EDS analyses of different Pt–Ru/C agglomerates show that the agglomerate chemical composition is not homogeneous. The analysed agglomerate compositions were in the range of $Pt_{50}Ru_{50}$ to $Pt_{40}Ru_{60}$.

5.2. TEM analysis on the aged MEA

Thin aged DMFC MEA cross-sections prepared by ultramicrotomy have been observed by TEM and compared to the fresh ones. Due to the huge heterogeneity of both the anode and cathode catalyst size in the fresh MEA, it was not possible to clearly

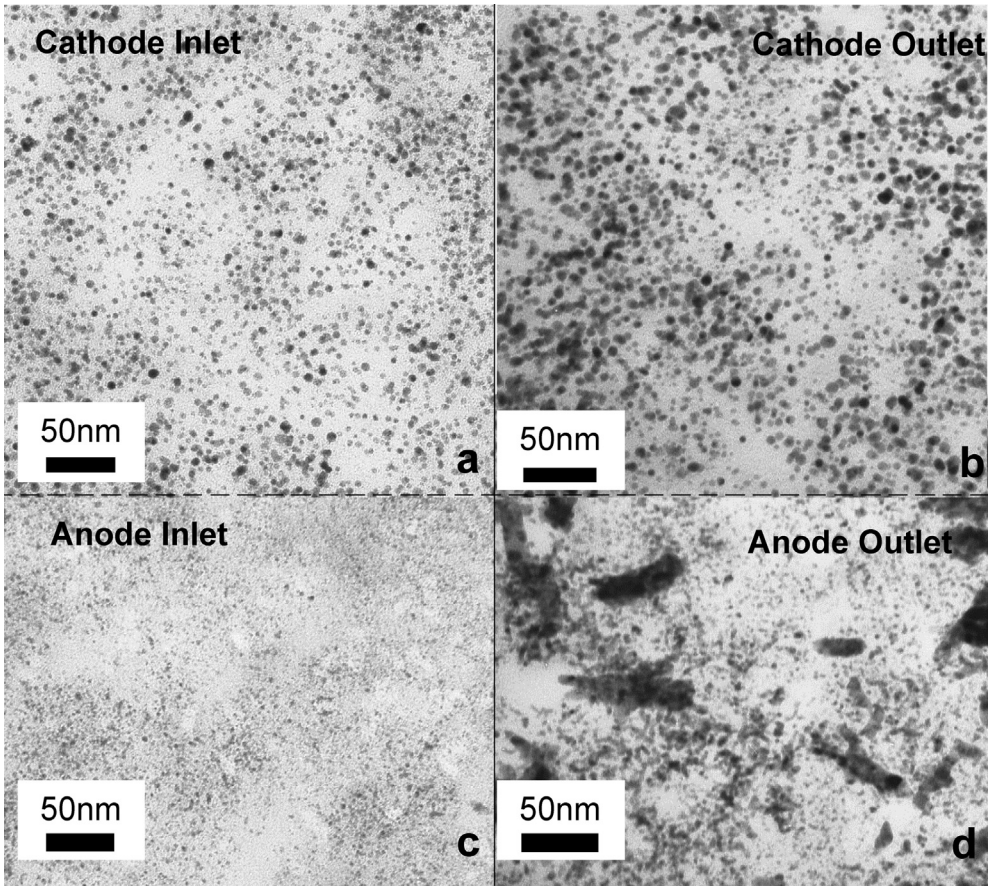

Fig. 7. TEM images of the Pt and Pt–Ru nanoparticles respectively in a) air inlet aged cathode, b) air outlet aged cathode, c) fuel inlet aged anode d) fuel outlet aged anode.

determine their size evolution. However, from a comparison of similar regions of reactants inlet and outlet zone, a slight average particle size increase in the cathode outlet seems to occur in comparison with cathode inlet, as showed in Fig. 7A and B, as well as at the anode, as in Fig. 7C and D.

EDS Ru and Pt elemental maps were acquired through the cathode. These maps (Fig. 8A–C) clearly reveal the presence of Ru in the cathode, confirming Ru cross-over already observed with XPS. The quantitative analyses of atomic concentrations provide a Ru:Pt ratio of (4 ± 1):(96 ± 1), which is lower than the corresponding ratio obtained by XPS (Ru:Pt ≈ 10:90). The reason may be the different surface sensitivities of XPS and X-EDS that are in the range of a few nm and hundreds of nm, respectively. Consequently, the higher relative concentration of Ru observed with XPS compared to X-EDX can suggest that Ru in fact covers the Pt particles as already spec-ulated above.

Moreover, a large number of small precipitates (around 10 nm) were observed within the membrane, in the zone located near the middle of the membrane cross-section. The EDS elemental map and spectra acquired on these precipitates, reported respectively in Fig. 8D and E, clearly indicates that they are Pt–Ru precipitates. In PEMFC aged under reformate, similar Pt–Ru precipitates were also observed within the membrane and a precipitate formation mechanism where Pt catalyses the Ru ion reduction by H_2 crossover within the membrane was suggested [36].

At the anode side, in some few zones of the MPL, some very small precipitates are detected. The X-EDS map, not shown for the sake of shortness, indicated that they are pure Ru precipitates. Ru diffusion toward the anode MPL could appear to be another anode degradation mechanism as it was observed in PEMFC aged under reformate [36]. In this sample, only few Ru precipitates are detected in the MPL near the anode catalyst layer and these precipitates were no more detectable farther (few μm far) from the anode catalyst layer. Consequently, these analyses are also in good agreement with XPS analysis which does not detect Ru precipitates in the anode MPL for this sample.

To summarize, microscopy analyses on the aged DMFC MEA show that the Pt/Ru anode catalysts are not stable under operation. Under the anode overpotential, Ru is oxidized into ions that could diffuse toward the membrane until the cathode and in the opposite direction toward the anode MPL. Some of the Ru ions are reduced within the membrane whereas a large quantity seems to be reduced within the cathode. Such a significant Ru crossover, more relevant than PEMFC one [36], is probably enhanced by the intense water flux through the MEA from anode to cathode already discussed.

6. Coupling in-situ and post-mortem analyses

After the long-term operation, the modification of the DMFC MEA components subjected to several permanent degradation mechanisms should have a relationship with the in-situ diagnostics presented in section 3.

From the TEM imaging and XPS results the cathode ECSA loss could be attributed to the combination of an average catalyst particle size increase, a loss of ionomer and Ru coverage of Pt nanoparticles, able to justify the measured reduction of cathode ECSA, especially in the reactants outlet region. The anode effectiveness

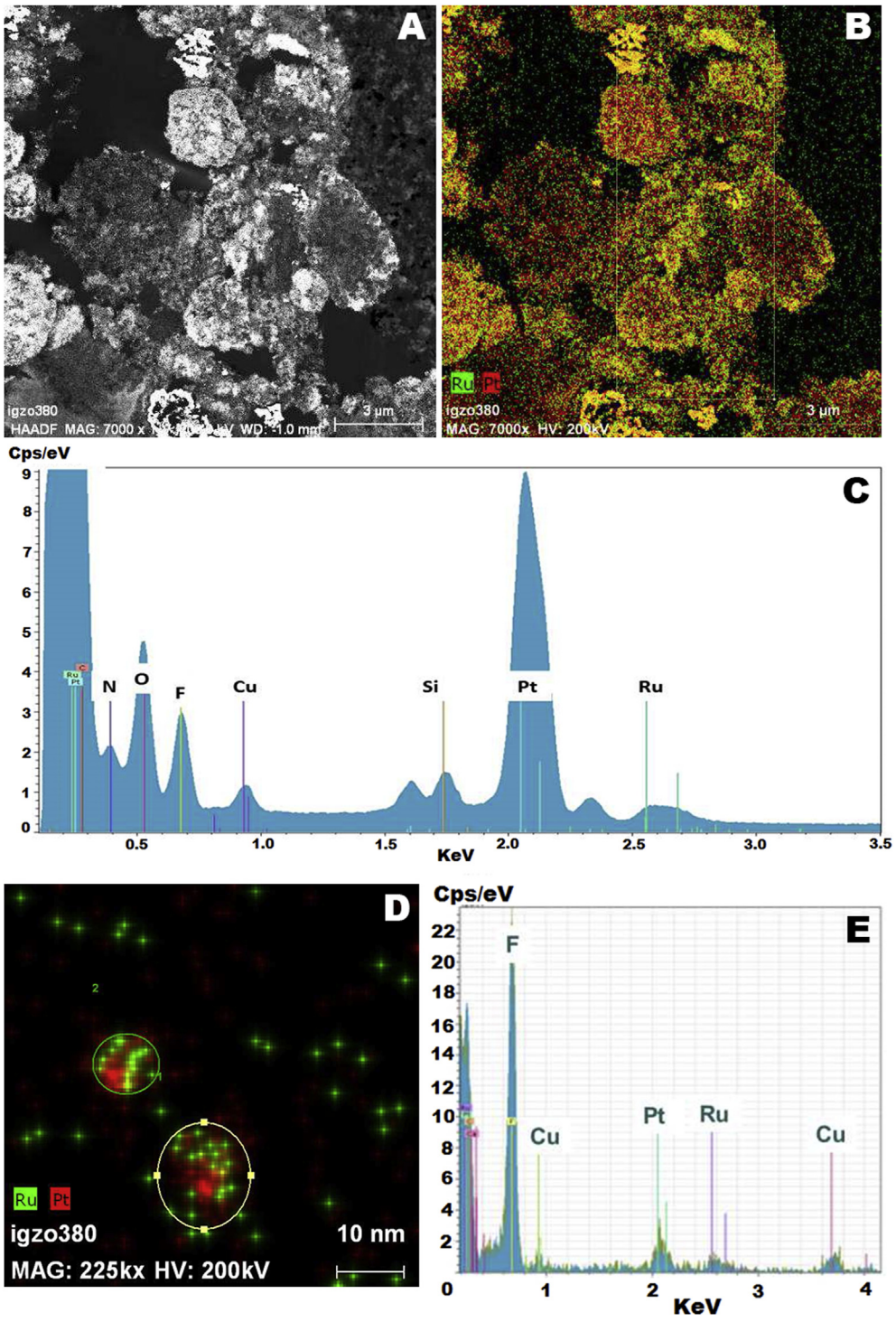

Fig. 8. Aged cathode catalyst layer: A) TEM image of the aged MEA CL. B) Pt and Ru EDS elemental map of the cathode catalyst layer. C) EDS spectra extracted from the elemental map that clearly indicated the presence of Ru at the cathode. Precipitates observed by TEM within the aged MEA membrane near the middle of the membrane cross-section: D) Pt (red) and Ru (green) X-EDS elemental map of these two precipitates. E) X-EDS spectra of the two precipitates obtained from the X-EDS map indicated that they are Pt–Ru precipitates. (For interpretation of the references to colour in this figure legend, the reader is referred to the web version of this article.)

loss could be due to a slight particle growth and a progressive ruthenium dissolution, that should result in a progressive increase of the anode overpotential, particularly at reactants outlet.

The considerable reduction of electrode ionomer content can also explain the increased mass transport resistance implying, in addition to the mentioned ECSA reduction, a variation of the catalyst layer morphology and properties, which affect locally water and gas fluxes and concentration. Moreover, the increase of mass transport resistance observed in polarization curves and impedance spectra can be also caused by the observed heterogeneous ECSA reduction that determines an increment of current and reactant flux in the healthiest region of the MEA, as reported in Ref. [50].

Membrane transport properties, evaluated also through methanol and water balances, result unaltered from the in-situ analysis. This suggests that the presence of nanoparticle precipitation within the membrane observed by TEM does not interfere with the membrane properties.

The negligible variations of both methanol and water fluxes are consistent with the XPS analyses performed on both anode and cathode GDL and MPL. Methanol and water fluxes are mainly regulated by MPL properties: the anode MPL presence determines a reduction of methanol crossover and a significant modification of water flux, while the cathode MPL presence has a major influence on water transport [62,63]. In the aged MEA, the overall transport properties remain constant, despite the severe degradation of anode GDL, because both anode and cathode MPL are not significantly degraded.

Finally, the effect of the ruthenium crossover on both cathode permanent and temporary degradation is still not explained in the literature; according to [64], since the platinum oxides formation is one of the most important cathode DMFC temporary degradation mechanisms [23,29], ruthenium can act as a promoter for the platinum oxides formation increasing the effects of such temporary degradation mechanism. However, the relationship between ruthenium crossover and DMFC temporary degradation still has to be investigated.

7. Conclusions

This work allowed to separate and quantify the effect of each component's degradation on voltage decay, distinguish the effects of active area loss at both at anode and cathode, mass transport issue, membrane decay and reversible degradation. Ex-situ analyses on pristine, activated and aged components allowed identifying the major degradation mechanisms and the related heterogeneities. The consistency of the results obtained from in-situ and ex-situ analyses permitted us to propose a solid interpretation of the major degradation mechanisms and quantify their effects on voltage decay, summarized below:

- *full refresh* procedure permits one to erase the temporary degradation allowing the quantification of permanent degradation. During the long term test, temporary and permanent degradation are respectively equal to 21 $\mu V\ h^{-1}$ and 59 $\mu V\ h^{-1}$;
- cathode ECSA decreases by 50% after 1100 h of operation and appears as the most important degradation mechanism; such high value, compared to PEMFC, is caused by cathode operation at high potential and high water content and flux. The effect of this ECSA reduction on performance decay is equal to 31 $\mu V\ h^{-1}$. This cathode electrode degradation is attributed by TEM and XPS analyses to an increase in catalyst particle size, especially at cathode outlet, Ru coverage of Pt nanoparticles and ionomer loss;
- anode electrode degradation, responsible for 9 $\mu V\ h^{-1}$, is related to ruthenium dissolution and migration to anode MPL and cathode CL, especially during the first hours of operation, as highlighted by both XPS and X-EDS techniques. The effect of ruthenium presence in cathode CL on both permanent and temporary degradation has to be further investigated;
- the EIS performed during the test confirms the increase of mass transport resistance, whose effect on voltage decay is about 15 $\mu V\ h^{-1}$. This can be explained by the observed reduction of ionomer content in the CLs and the heterogeneous ECSA reduction.
- membrane degradation is limited and gives a minor contribution to voltage decay, about 4 $\mu V\ h^{-1}$, even though core–shell Pt/Ru precipitates have been observed within the membrane.

Further work will be dedicated to evaluate how much the observed degradation mechanisms are influenced by operating conditions.

Acknowledgements

The research leading to these results has received funding from the European Union's Seventh Framework Program (FP7/2007-2013) for the Fuel Cells and Hydrogen Joint Technology Initiative under grant agreement n°256776 (FCH-JU project Premium Act) and n°621216 (FCH-JU project Second Act).

Appendix

A1. Minimization of temporary degradation

Despite the *refresh* cycles operating strategy used for DMFC operation (described in section 2.2) is very effective in comparison with others, as investigated in Ref. [39], it does not permit to completely avoid the temporary degradation during cell operation. An operation interruption for diagnostics, already after few tens of hours of *refresh* cycles operation, allows a noticeably higher performance recovery than the usual *refresh* cycles procedure. This confirms that the adopted operating strategy does not avoid temporary degradation accumulation, whose minimization can only be obtained during a long operation interruption.

An innovative *full refresh* technique has been appositely developed in order to get the highest performance recovery. It has been applied during the degradation tests just before and after the diagnostic measurements, in order to reveal only the permanent component of DMFC degradation and to ensure its calculation method reliability. The *full refresh* consists in 16 h of methanol solution continuous circulation in the anode serpentine at very low mass flow (0.33 g min^{-1}), while both cathode distributor inlet and outlet are plugged to avoid oxygen infiltrations and the temperature is maintained at 75 °C.

During this long interruption, anode GDL and CL saturation increases due to progressive hydration, resulting in optimal anode performances when the operation restarts, consistently with [30]. The electrolytic membrane gets fully hydrated resulting in low ohmic resistance. Furthermore, cathode potential progressively reduces to about 0 V: this has a strong positive effects on DMFC performances, probably related to platinum oxides reduction [29].

The *full refresh* positive effect on performances has been proved on a DMFC MEA activated with the manufacturer suggested procedure,[3] by applying the *full refresh* at the end of the activation. The voltage value obtained after the *full refresh* interruption is higher than the one at the BoL, confirming that it permits to minimize temporary degradation effects. For this reason, *full refresh* can be also helpful to reduce DMFC activation procedure duration.

The impedance spectra analysis, here not reported for the sake of shortness, acquired before and after the *full refresh* interruption confirm some of the reasons of its effectiveness on DMFC performances. The analysis points out a decrease of membrane ohmic resistance, which can be related to the higher membrane hydration determined by *full refresh.* Moreover, the cell total resistance diminishes consistently with the observed performance gain.

Thus, the activation procedure used in this work to reach the BoL performance, consists in a 3 days' procedure, interspersed by *full refresh* cycles, including current ramps till the reference current.

[3] The details cannot be provided for confidential agreement.

References

[1] S.K. Kamarudin, F. Achmad, et al., Overview on the application of direct methanol fuel cell (DMFC) for portable electronic devices, Int. J. Hydrogen Energy 34 (2009) 6902–6916.

[2] P. Agnolucci, Economics and market prospects of portable fuel cells, Int. J. Hydrogen Energy 32 (2007) 4319–4328.

[3] X. Li, A. Faghri, Review and advances of direct methanol fuel cells (DMFCs) part I: design, fabrication, and testing with high concentration methanol solutions, J. Power Sources 226 (2013) 223–240.

[4] S.C. Thomas, X. Ren, P. Zelenay, Direct methanol fuel cells: progress in cell performance and cathode research, Electrochim. Acta 47 (2002) 3741–3748.

[5] H. Liu, C. Song, L. Zhang, J. Zhang, H. Wang, D.P. Wilkinson, A review of anode catalysis in the direct methanol fuel cell, J. Power Sources 155 (2006) 95–110.

[6] C. Cremers, M. Scholz, et al., Developments for improved direct methanol fuel cell stacks for portable power, Fuel Cells 7 (2007) 21–31.

[7] A. Arico, S. Srinivasan, V. Antonucci, DMFCs: from fundamental aspects to technology development, Fuel Cells 1 (2001) 133–161.

[8] Q. Lai, G. Yin, Z. Wang, C. Du, P. Zuo, X. Cheng, Influence of methanol crossover on the fuel utilization of passive direct methanol fuel cell, Fuel Cells 8 (2008) 399–403.

[9] V. Gogel, T. Frey, Z. Yongsheng, K.A. Friedrich, L. Jorissen, J. Garche, Performance and methanol permeation of direct methanol fuel cells: dependence on operating conditions and on electrode structure, J. Power Sources 127 (2004) 172–180.

[10] S. Yoon, G. Hwang, W. Cho, I. Oh, S. Hong, H. Ha, Modification of polymer electrolyte membranes for DMFCs using Pd films formed by sputtering, J. Power Sources 106 (2002) 215–223.

[11] B. Krishnamurthy, S. Deepalochani, K. Dhathathreyan, Effect of ionomer content in anode and cathode catalyst layers on direct methanol fuel cell performance, Fuel Cells 8 (2008) 404–409.

[12] A. Aricò, P. Cretì, E. Modica, G. Monforte, V. Baglio, V. Antonucci, Investigation of direct methanol fuel cells based on unsupported Pt–Ru anode catalysts with different chemical properties, Electrochim. Acta 45 (2000) 4319–4328.

[13] J. Park, J. Kim, Y. Seo, D. Yu, H. Cho, S. Bae, Operating temperature dependency on performance degradation of direct methanol fuel cells, Fuel Cells 12 (2012) 426–438.

[14] J. Prabhuram, N.N. Krishnan, B. Choi, T. Lim, H.Y. Ha, S. Kim, Long-term durability test for direct methanol fuel cell made of hydrocarbon membrane, Int. J. Hydrogen Energy 35 (2010) 6924–6933.

[15] J. Liu, Z. Zhou, X. Zhao, Q. Xin, G. Sun, B. Yi, Studies on performance degradation of a direct methanol fuel cell (DMFC) in life test, Chem. Phys. 6 (2004) 134–137.

[16] Z. Wang, H. Rivera, X. Wang, H. Zhang, P. Feng, E.A. Lewis, E.S. Smotkin, Catalyst failure analysis of a direct methanol fuel cell membrane electrode assembly, J. Power Sources 177 (2008) 386–392.

[17] L.S. Sarma, C. Chen, G. Wang, K. Hsueh, C. Huang, H. Sheu, D. Liu, J. Lee, B. Hwang, Investigations of direct methanol fuel cell (DMFC) fading mechanisms, J. Power Sources 167 (2007) 358–365.

[18] J. Park, J. Lee, J. Sauk, I. Son, The operating mode dependence on electrochemical performance degradation of direct methanol fuel cells, Int, J. Hydrogen Energy 33 (2008) 4833–4843.

[19] Y. Tian, G. Sun, Q. Mao, S. Wang, H. Liu, Q. Xin, In situ analysis on water transport in a direct methanol fuel cell durability test, J. Power Sources 185 (2008) 1015–1021.

[20] P. Liu, G. Yin, K. Cai, Investigation on cathode degradation of direct methanol fuel cell, Electrochim. Acta 54 (2009) 6178–6183.

[21] A. Mehmood, M.A. Scibioh, J. Prabhuram, M. An, H.Y. Ha, A review on durability issues and restoration techniques in long-term operations of direct methanol fuel cells, J. Power Sources 297 (2015) 224–241.

[22] H. Cha, C. Chen, J. Shiu, Investigation on the durability of direct methanol fuel cells, J. Power Sources 192 (2009) 451–456.

[23] C. Eickes, P. Piela, J. Davey, P. Zelenay, Recoverable cathode performance loss in direct methanol fuel cells, J. Electrochem. Soc. 153 (2006) A171–A178.

[24] J. Park, M.A. Scibioh, S. Kim, H. Kim, I. Oh, T.G. Lee, H.Y. Ha, Investigations of performance degradation and mitigation strategies in direct methanol fuel cells, Int. J. Hydrogen Energy 34 (2009) 2043–2051.

[25] Q. Ye, T.S. Zhao, Electrolytic hydrogen evolution in DMFCs induced by oxygen interruptions and its effect on cell performance, Electrochem. Solid State Lett. 8 (2005) A211–A214, http://dx.doi.org/10.1149/1.1869012.

[26] D.U. Sauer, T. Sanders, B. Fricke, T. Baumhofer, K. Wippermann, A.A. Kulikovsky, H. Schmitz, J. Mergel, Measurement of the current distribu-tion in a direct methanol fuel cell—confirmation of parallel galvanic and electrolytic operation within one cell, J. Power Sources 176 (2008) 477–483.

[27] C. Chen, H. Cha, Strategy to optimize cathode operating conditions to improve the durability of a direct methanol fuel cell, J. Power Sources 200 (2012) 21–28.

[28] N. Wongyao, A. Therdthianwong, S. Therdthianwong, S.M. Senthil Kumar, K. Scott, A comparison of direct methanol fuel cell degradation under different modes of operation, Int. J. Hydrogen Energy 38 (2013) 9464–9473.

[29] F. Bresciani, C. Rabissi, A. Casalegno, M. Zago, R. Marchesi, Experimental investigation on DMFC temporary degradation, Int. J. Hydrogen Energy 39 (2014) 21647–21656.

[30] F. Bresciani, A. Casalegno, M. Zago, R. Marchesi, A parametric analysis on DMFC anode degradation, Fuel Cells 14 (2014) 386–394.

[31] A. Casalegno, F. Bresciani, M. Zago, R. Marchesi, Experimental investigation of methanol crossover evolution during direct methanol fuel cell degradation tests, J. Power Sources 249 (2014) 103–109.

[32] X. Cheng, C. Peng, M. You, L. Liu, Y. Zhang, Q. Fan, Characterization of catalysts and membrane in DMFC lifetime testing, Electrochim. Acta 51 (2006) 4620–4625.

[33] L. Guetaz, S. Escribano, O. Sicardy, Study by electron microscopy of proton exchange membrane fuel cell membrane-electrode assembly degradation mechanisms: influence of local conditions, J. Power Sources 212 (2012) 169–178.

[34] S.J. Bae, S. Kim, S. Um, J. Park, J. Lee, H. Cho, A prediction model of degradation rate for membrane electrode assemblies in direct methanol fuel cells, Int. J. Hydrogen Energy 34 (2009) 5749–5758.

[35] P. Hartmann, D. Gerteisen, Local degradation analysis of a real long-term operated DMFC stack MEA, J. Power Sources 219 (2012) 147–154.

[36] P.A. Henry, L. Guétaz, N. Pélissier, P. Jacques, S. Escribano, Structural and chemical analysis by transmission electron microscopy of Pt–Ru membrane precipitates in proton exchange membrane fuel cell aged under reformate, J. Power Sources 275 (2015) 312–321.

[37] A. Casalegno, R. Marchesi, DMFC performance and methanol cross-over: experimental analysis and model validation, J. Power Sources 185 (2008) 318–330.

[38] S.J. Bae, S. Kim, J.I. Park, J. Lee, H. Cho, J. Park, Lifetime prediction through accelerated degradation testing of membrane electrode assemblies in direct methanol fuel cells, Int. J. Hydrogen Energy 35 (2010) 9166–9176.

[39] F. Bresciani, A. Casalegno, J.L. Bonde, M. Odgaard, R. Marchesi, A comparison of operating strategies to reduce DMFC degradation, Int. J. Energy Res. 38 (2014) 117–124.

[40] S.K. Roy, M.E. Orazem, Error analysis of the impedance response of PEM fuel cells, J. Electrochem. Soc. 154 (2007) B883–B891.

[41] E. Barsoukov, J.R. Macdonald, Impedance Spectroscopy: Theory, Experiment, and Applications, John Wiley & Sons, 2005.

[42] H. Wang, X. Yuan, H. Li, PEM Fuel Cell Diagnostic Tools, CRC press, 2011.

[43] S. Galbiati, A. Baricci, A. Casalegno, R. Marchesi, Degradation in phosphoric acid doped polymer fuel cells: A 6000 h parametric investigation, Int. J. Hydrogen Energy 38 (2013) 6469–6480.

[44] P. Gazdzicki, I. Biswas, M. Schulze, Methodic aspects of XPS depth profiling for investigations of fuel cell components, Surf. Interface Anal. 46 (2014) 350–356.

[45] Y. Shao-Horn, W. Sheng, S. Chen, P. Ferreira, E. Holby, D. Morgan, Instability of supported platinum nanoparticles in low-temperature fuel cells, Top. Catal. 46 (2007) 285–305.

[46] M. Zago, A. Casalegno, C. Santoro, R. Marchesi, Water transport and flooding in DMFC: experimental and modeling analyses, J. Power Sources 217 (2012) 381–391.

[47] A.A. Kulikovsky, A model for DMFC cathode impedance: the effect of methanol crossover, Electrochem. Commun. 24 (2012) 65–68.

[48] M. Zago, A. Casalegno, F. Bresciani, R. Marchesi, Effect of anode MPL on water and methanol transport in DMFC: experimental and modeling analyses, Int. J. Hydrogen Energy 39 (2014) 21620–21630.

[49] T. Zhao, C. Xu, R. Chen, W. Yang, Mass transport phenomena in direct methanol fuel cells, Prog. Energy Combust. 35 (2009) 275–292.

[50] A. Baricci, A Combined Experimental and Modelling Approach for the Improved Characterization of High Temperature PEM Fuel Cell, PhD Thesis, Politecnico di Milano, 2015.

[51] M. Schulze, K.A. Friedrich, Relations of water management and degradation processes in PEFC, ECS Trans. 12 (2008) 101–111.

[52] M. Schulze, C. Christenn, XPS investigation of the PTFE induced hydrophobic properties of electrodes for low temperature fuel cells, Appl. Surf. Sci. 252 (2005) 148–153.

[53] M. Schulze, M. Lorenz, T. Kaz, XPS study of electrodes formed from a mixture of carbon black and PTFE powder, Surf. Interface Anal. 34 (2002) 646–651.

[54] M. Schulze, K. Bolwin, E. Gülzow, W. Schnurnberger, XPS analysis of PTFE decomposition due to ionizing radiation, Fresenius J. Anal. Chem. 353 (1995) 778–784.

[55] G. Park, C. Pak, Y. Chung, J. Kim, W.S. Jeon, Y. Lee, K. Kim, H. Chang, D. Seung, Decomposition of Pt–Ru anode catalysts in direct methanol fuel cells, J. Power Sources 176 (2008) 484–489.

[56] Y. Chung, C. Pak, G. Park, W.S. Jeon, J. Kim, Y. Lee, H. Chang, D. Seung, Understanding a degradation mechanism of direct methanol fuel cell using TOF-SIMS and XPS, J. Phys. Chem. C 112 (2008) 313–318.

[57] S. Tanuma, C.J. Powell, D.R. Penn, Calculations of electron inelastic mean free paths. II. Data for 27 elements over the 50–2000 eV range, Surf. Interface Anal. 17 (1991) 911–926.

[58] P. Piela, C. Eickes, E. Brosha, F. Garzon, P. Zelenay, Ruthenium crossover in direct methanol fuel cell with Pt-Ru black anode, J. Electrochem. Soc. 151 (2004) A2053–A2059.

[59] D. Clark, W. Brennan, An ESCA investigation of low energy electron beam interactions with polymers: II. PVDF and a mechanistic comparison between PTFE and PVDF, J. Electron Spectrosc. Relat. Phenom. 47 (1988) 93–104.

[60] D. Briggs, High Resolution XPS of Organic Polymers: the Scienta ESCA300 Database, Wiley, 1992.

[61] D. Clark, W. Feast, D. Kilcast, W. Musgrave, Applications of ESCA to polymer chemistry. III. Structures and bonding in homopolymers of ethylene and the

fluoroethylenes and determination of the compositions of fluoro copolymers, J. Polym. Sci. Polym. Chem. Ed. 11 (1973) 389–411.
[62] A. Casalegno, C. Santoro, F. Rinaldi, R. Marchesi, Low methanol crossover and high efficiency direct methanol fuel cell: the influence of diffusion layers, J. Power Sources 196 (2011) 2669–2675.
[63] F. Bresciani, C. Rabissi, M. Zago, R. Marchesi, A. Casalegno, On the effect of gas diffusion layers hydrophobicity on direct methanol fuel cell performance and degradation, J. Power Sources 273 (2015) 680–687.
[64] D. Dixon, K. Wippermann, J. Mergel, A. Schoekel, S. Zils, C. Roth, Degradation effects at the methanol inlet, outlet and center region of a stack MEA operated in DMFC, J. Power Sources 196 (2011) 5538–5545.